Core structures of vortices in Ginzburg-Landau theory for neutron $^3P_2$ superfluids

Michikazu Kobayashi
School of Environmental Science and Engineering, Kochi University of Technology, Miyanoguchi 185, Tosayamada, Kami, Kochi 782-8502, Japan

Muneto Nitta
Department of Physics, and Research and Education Center for Natural Sciences, Keio University, Hiyoshi 4-1-1, Yokohama, Kanagawa 223-8521, Japan

(Received 6 January 2022; accepted 15 March 2022; published 28 March 2022)

We investigate vortex solutions in the Ginzburg-Landau theory for neutron $^3P_2$ superfluids relevant for neutron star cores in which neutron pairs possess the total angular momentum $J = 2$ with spin triplet and P wave, in the presence of the magnetic field parallel to the angular momentum of vortices. The ground state is known to be in the uniaxial nematic (UN) phase in the absence of magnetic field, while it is in the D_2 (D_4) biaxial nematic (BN) phase in the presence of the magnetic field below (above) the critical value. We find that a singly quantized vortex always splits into two half-quantized non-Abelian vortices connected by soliton(s) as a vortex molecule with any strength of the magnetic field. In the UN phase, two half-quantized vortices with ferromagnetic cores are connected by a linear soliton with the D_4 BN order. In the D_2 (D_4) BN phase, two half-quantized vortices with cyclic cores are connected by three linear solitons with the D_4 (D_2) BN order. The energy of the vortex molecule monotonically increases and the distance between the two half-quantized vortices decreases with the magnetic field increases, except for a discontinuously increasing jump of the distance at the critical magnetic field. We also construct an isolated half-quantized non-Abelian vortex in the D_4 BN phase.

DOI: 10.1103/PhysRevC.105.035807

I. INTRODUCTION

Pulsars or rapidly rotating neutron stars are dense and compact stars under extreme conditions, thereby serving as astrophysical laboratories for studying nuclear and QCD matter at high density, with a strong magnetic field and under rapid rotation [1,2]. The recent progress in astrophysical observations promote us to study the interiors of neutron stars more precisely: the observation of massive neutron stars whose masses are about twice as large as the solar mass [3,4], the gravitational waves from a binary neutron star merger [5,6], and the Neutron Star Interior Composition Explorer (NICER) mission [7,8], expected to reveal interior states of neutron stars.

The interior of neutron stars is believed to exhibit neutron superfluidity and proton superconductivity as first predicted by Migdal [9] (see Refs. [1,10–14] for recent reviews). Such superfluid and superconducting components can alter low-energy excitation modes compared with the normal phase, and thus their existence can affect several processes and properties of neutron stars, such as neutrino emissivities and specific heats relevant to the long relaxation time after the sudden speed-up events, that is pulsar glitches, of neutron stars [15–17], and the enhancement of neutrino emission around the critical point of the superfluid transition [18–23]. The neutron superfluids are realized by the attraction between two neutrons in the $^1S_0$ channel at the low density [9]. It was, however, shown in Ref. [24] that this channel is repulsive at higher densities as a consequence of the strong short-range repulsion. Thus, it was proposed that neutron $^3P_2$ superfluids, in which neutron pairs possess the total angular momentum $J = 2$ with spin triplet and P wave, are more relevant at higher density [25–42]. The $^3P_2$ interaction originates from a strong spin-orbit force at large scattering energy, and thus the neutron $^3P_2$ superfluids are expected to be realized in the high-density regions in the inner cores of neutron stars. They also can survive in neutron stars with strong magnetic fields, such as magnetars with the magnetic field 10^{15}–10^{18} G, since they are tolerant against the strong magnetic field due to the fact that the aligned pairs of Cooper pairs with the spin-triplet pairing are not broken by the Zeeman effect. In the S-wave case, it has also predicted that Cooper pairs can survive at around the magnetic field 10^{17} G [43].

In astrophysical observations, the possibility of the existence of neutron $^3P_2$ superfluids inside neutron stars are investigated; the rapid cooling of the neutron star in Cassiopeia A might be explained by the enhancement of neutrino emissivities due to the formation and dissociation of neutron $^3P_2$ Cooper pairs [21–23].

On the other hand, as the theoretical aspects are concerned, neutron $^3P_2$ superfluids have rich topological structures both

TABLE I. In the absence and presence of the magnetic field below and above the critical value B_c, (a) phases, (b) unbroken symmetries, (c) OPMs, (d) the first homotopy groups of the OPMs, (e) the order inside half-quantized vortex cores, (f) the number of solitons connecting the two half-quantized vortices, and (g) the order inside soliton cores are summarized. Here, $\mathbb{Q} = D_2^*$ is a quaternion group with $*$ implying the universal covering group. $\rtimes_h$ is a product defined in Ref. [93], ensuring the existence of isolated half-quantized non-Abelian vortices. (e), (f), and (g) are new results presented in this paper.

$\lvert\boldsymbol{B}\rvert$	$\lvert\boldsymbol{B}\rvert = 0$	$0 < \lvert\boldsymbol{B}\rvert < B_c$	$B_c < \lvert\boldsymbol{B}\rvert$
(a) Phase	UN	D_2 BN	D_4 BN
(b) Symmetry	$O(2)$	D_2	D_4
(c) OPM	$S^1 \times \mathbb{R}P^2$	$U(1) \times \frac{SO(3)}{D_2}$	$\frac{U(1) \times SO(3)}{D_4}$
(d) π_1(OPM)	$\mathbb{Z} \oplus \mathbb{Z}_2$	$\mathbb{Z} \oplus \mathbb{Q}$	$\mathbb{Z} \rtimes_h D_4^*$
(e) Vortex core order	Ferro	Cyclic	Cyclic
(f) # of solitons	1	3	3
(g) Soliton core order	D_4 BN	D_4 BN	D_2 BN

in bosonic and fermionic excitations. There are basically two related approaches for theoretical study of superfluids. The most fundamental theory is the Bogoliubov-de Gennes (BdG) equation offering a framework to deal with fermion degrees of freedom. The other is the Ginzburg-Landau (GL) approach as the low-energy effective theory obtained by integrating out fermion degrees of freedom, which is an expansion of both the order parameters and spatial derivatives, and thus is valid only in the region close to the critical temperature. The BdG approach was applied to $^3P_2$ superfluids and the phase diagram in the plane of the temperature and magnetic field was obtained [44]. Furthermore, $^3P_2$ superfluids were shown to be topological superfluids of a class DIII in the classification of topological insulators and superconductors [45,46], allowing a topologically protected gapless Majorana fermion on its boundary [44]. On the other hand, within the GL theory, superfluid states with $J = 2$ are in general classified into nematic, cyclic, and ferromagnetic phases etc. [47]. The GL theory for $^3P_2$ superfluids was obtained [30,31,48–56], and in the weak coupling limit, the nematic phase was found to be the ground state of $^3P_2$ superfluids [48–50]. The nematic phase consists of three subphases with different unbroken symmetries: uniaxial nematic (UN), D_2 biaxial nematic (D_2 BN), and D_4 biaxial nematic (D_4 BN) phases, with unbroken groups $O(2)$, D_2 and D_4, respectively, where D_n is a dihedral group of order n [see Table I(a) and I(b)]. Corresponding order parameter manifolds (OPMs) are $U(1) \times SO(3)/O(2) \simeq S^1 \times \mathbb{R}P^2$, $U(1) \times SO(3)/D_2$, and $[U(1) \times SO(3)]/D_4$, respectively [see Table I(c)]. These are continuously degenerated in the absence of magnetic field in the GL expansion up to the fourth order.[1] In the presence of the magnetic field and/or with the inclusion of the sixth-order term into the GL theory, the continuous degeneracy is lifted to pick up either UN, D_2 BN, or D_4 BN state as the ground state for zero magnetic field, nonzero one below the critical value B_c, and nonzero one above B_c, respectively [52,54,55] [see Table I(a)]. There is a subtle problem on the instability of the ground states for large value of the order parameter, which is cured by the expansion up to the eighth order [56]. The phase diagram up to the eighth order captures the essential features of that determined in the BdG equation [44], including a tricritical point connecting first- and second-order phase transition lines between D_4 and D_2 BN phases [44,57]. Apart from nematic phases, more general uniform states of $^3P_2$ superfluids were classified [58], which is also useful to identify local states such as vortex cores. As a uniform ground state, the ferromagnetic state is in fact found to appear, beyond the quasiclassical approximation, in the region close to the critical temperature [59]. The GL approach is useful to deal with bosonic collective excitations and topological defects. Bosonic excitations in the $^3P_2$ superfluids yield collective modes [60–72] relevant, for instance, for cooling process of neutron stars. Topological defects such as domain walls [73] and the boundary defect (boojums) of $^3P_2$ superfluids [74] were investigated.

One of the most salient features of superfluidity is the fact that circulations of vortices are quantized so that the wave function is single valued around the vortices (the Feynman-Onsager's quantization), yielding the existence of quantized vortices. When a superfluid is rotating, a vortex lattice is formed as observed in helium superfluids and ultracold atomic gasses. In the context of superfluids in neutron stars, the origin of pulsar glitches was proposed to be explained by sudden releases of a large number of quantized vortices [75,76]. In the case of $^3P_2$ superfluids, quantized vortices were investigated both in the GL theory [30,49,50,52,53,77] (see also Ref. [78] for coreless vortices), and in the BdG theory [79,80]. The first homotopy group classifying vortices is given in Ref. [52] [see Table I(d)]. Singly quantized vortices in $^3P_2$ superfluids were studied in the GL theory [30,49,50,52,77], and topologically protected Majorana fermions in the vortex core were found in the BdG theory [79]. Vortices more peculiar to the $^3P_2$ superfluids are half-quantized non-Abelian vortices, which are allowed only in the D_4 BN phase [53,80]. Their circulations are a half of the Feynman-Onsager's quantized circulations, and the first homotopy group characterizing these vortices is non-Abelian, thus giving noncommutativity of exchanging vortices. The existence of half-quantized vortices was proposed to explain a scaling law of pulsar glitches [81]. In Ref. [80], it was found in the BdG formalism that a singly quantized vortex is split into two half-quantized non-Abelian vortices. It was also found that a Majorna fermion zero mode is trapped in each half-quantized vortex.

Apart from $^3P_2$ superfluids, spin-2 spinor ultracold atomic Bose-Einstein condensates (BECs) are also $J = 2$ condensates whose ground states are possibly nematic phase [58,82–86] sharing almost the same bosonic properties with $^3P_2$ superfluids, thus admitting the same order parameter manifold and non-Abelian half-quantized vortices [85,86]. Therefore, studying bosonic properties of $^3P_2$ superfluids is also applicable to spin-2 BECs, which can be experimentally testable in principle, although the current experiments of ^{87}Rb

[1] More precisely these are connected by a parameter of continuous degeneracy called a quasi-Nambu-Goldstone mode [85], and these OPMs are submanifolds of an extended OPM $(S^1 \times S^4)/\mathbb{Z}_2$.

atoms imply their ground state to be in the cyclic or nematic phase [87–92].

In this paper, we investigate vortex solutions, namely singly quantized vortices and half-quantized non-Abelian vortices, in neutron $^3P_2$ superfluids within the GL approach. The orientation of the magnetic field is fixed to be parallel to the angular momentum of vortices. In the previous studies of vortices in the GL theory, an axial symmetry around the vortex axis was assumed [30,49,50,52,53,77]. In contrast, imposing no axial symmetry, we find that a singly quantized vortex always splits into two half-quantized non-Abelian vortices with any strength of the magnetic field. An advantage to use the GL theory compared with the BdG equation employed in Ref. [79] is that we do not have to consider the direction of splitting *a priori*. In the UN phase with the zero magnetic field, cores of two half-quantized vortices are found to be filled with the ferromagnetic states, while they are filled with the cyclic states in the D_2 and D_4 BN phases in the presence of the magnetic field, as summarized in Table I(e). In the UN phase, the two half-quantized vortices are connected by a single soliton of the D_4 BN order while they are connected by three linear solitons with the D_4 (D_2) BN order in the D_2 (D_4) BN phase, as summarized in Table I(f) and I(g). The appearance of the D_4 BN order around the vortex core in the UN and D_2 BN phases is a consequence of the fact that isolated half-quantized vortices can topologically exist only in the D_4 BN state. We also show that the energy of the vortex molecule monotonically increases as the magnetic field increases, which is continuous everywhere including the critical magnetic field separating D_2 and D_4 BN states. On the other hand, the distance between the two half-quantized vortices decreases with the magnetic field increases, except for a discontinuously increasing jump at the critical magnetic field. We also construct an isolated half-quantized non-Abelian vortex in the D_4 BN phase above the critical magnetic field.

A molecule of half-quantized vortices connected by a soliton or domain wall can be found in various systems such as multicomponent or multigap superconductors [94–106], coherently coupled multicomponent BECs [107–122], dense QCD of quark matter [123], and the two-Higgs doublet model [124] as a model beyond the standard model of elementary particles. Compared with these systems, the unique feature of $^3P_2$ superfluids is that constituent half-quantized vortices are non-Abelian vortices, that is, characterized by a non-Abelian first homotopy group.

This paper is organized as follows. In Sec. II, we begin with formulations of $^3P_2$ superfluids within the GL approach in our notation. Section III shows our numerical results for vortex states in the $^3P_2$ superfluids. Section IV is devoted to a summary and discussion.

II. GINZBURG-LANDAU FREE ENERGY FOR $^3P_2$ NEUTRON SUPERFLUIDS

We start from a brief review of the GL theory for $^3P_2$ superfluids [56] reformulated in the notation of Ref. [58]. The effective GL Lagrangian density f is given by

$$f = K_0\left(f_{202}^{(0)} + f_{202}^{(1)}\right) + \alpha f_{002} + \beta_0 f_{004} + \gamma_0 f_{006} + \delta_0 f_{008} + \beta_2 f_{022} + \gamma_2 f_{024} + \sum_{4l+2m+n=10} O(\nabla^l |\boldsymbol{B}|^m A^n), \tag{1}$$

where f_{lmn} is the free energy part including l spatial derivatives ∇, mth order of the magnetic field $\boldsymbol{B}$, and nth order of spin-2 spinor order parameter $\psi = (\psi_2, \psi_1, \psi_0, \psi_{-1}, \psi_{-2})^T$. The spatial derivative term f_{202} is further separated into current-spin-independent and -dependent parts $f_{202}^{(0)}$ and $f_{202}^{(1)}$, respectively. Their specific forms can be written as

$$\begin{aligned}
f_{202}^{(0)} &= 3\boldsymbol{j}^\dagger \cdot \boldsymbol{j}, \\
f_{202}^{(1)} &= 4\boldsymbol{j}^\dagger \cdot \boldsymbol{j} - \frac{i}{2}\boldsymbol{j}^\dagger \cdot \hat{\boldsymbol{S}} \times \boldsymbol{j} - (\boldsymbol{j}^\dagger \cdot \hat{\boldsymbol{S}})(\hat{\boldsymbol{S}} \cdot \boldsymbol{j}), \\
f_{002} &= 3\rho, \\
f_{004} &= 6\rho^2 + \frac{3}{4}\boldsymbol{S}^2 - \frac{3}{2}|\Psi_{20}|^2, \\
f_{006} &= -324\rho^3 - 81\rho\boldsymbol{S}^2 + 162\rho|\Psi_{20}|^2 + 15|\Psi_{30}|^2 - 27|\Phi_{30}|^2, \\
f_{008} &= 6480\rho^4 + 1944\rho^2\boldsymbol{S}^2 - 5184\rho^2|\Psi_{20}|^2 - 864\rho|\Psi_{30}|^2 + 2592\rho|\Phi_{30}|^2 + 81\boldsymbol{S}^4 + 648|\Psi_{20}|^4 - 1296\Gamma_4 \\
f_{022} &= 2\rho\boldsymbol{B}^2 - \frac{1}{2}\psi^\dagger \hat{S}_{\boldsymbol{B}} \hat{S}_{\boldsymbol{B}} \psi, \\
f_{024} &= \left(-106\rho^2 + \frac{9}{2}\boldsymbol{S}^2 + 31|\Psi_{20}|^2\right)\boldsymbol{B}^2 + \left(22\rho\psi^\dagger \hat{S}_{\boldsymbol{B}} \hat{S}_{\boldsymbol{B}} \psi + \mathrm{Re}\left[\Psi_{20}^* \psi^T \hat{S}_{\boldsymbol{B}}^T \hat{T} \hat{S}_{\boldsymbol{B}} \psi\right] + \frac{5}{4}\Psi_{22}^\dagger \hat{S}_{\boldsymbol{B}} \hat{S}_{\boldsymbol{B}} \Psi_{22} + \frac{1}{2}\Phi_{22}^T \hat{S}_{\boldsymbol{B}}^T \hat{T} \hat{S}_{\boldsymbol{B}} \Phi_{22}\right),
\end{aligned} \tag{2}$$

where $\hat{S}_i$ ($i = x, y, z$) are 5×5 spin-2 matrices, $\hat{T}$ is the time-reversal operator defined by $(\hat{T}\psi)_m \equiv (-1)^m \psi_{-m}$, and $\hat{S}_{\boldsymbol{B}} \equiv \hat{\boldsymbol{S}} \cdot \boldsymbol{B}$. The ψ-dependent terms $\boldsymbol{j}$, ρ, $\boldsymbol{S}$, Ψ_{20}, Ψ_{30}, Φ_{30}, Γ_4 are defined by

$$
\begin{aligned}
&\boldsymbol{j} = -i\nabla\psi, \quad \rho = \psi^\dagger\psi, \quad \boldsymbol{S} = \psi^\dagger\hat{\boldsymbol{S}}\psi,\\
&\Psi_{20} = \psi^T\hat{T}\psi = \sqrt{5}\sum_{m_1,m_2=-2}^{2} C^{00}_{2m_1,2m_2}\psi_{m_1}\psi_{m_2},\\
&\Psi_{30} = -\sqrt{\frac{35}{2}}\sum_{J=0}^{4}\sum_{M=-J}^{J}\sum_{m_1,m_2,m_3=-2}^{2}\\
&\qquad\times C^{00}_{JM,2m_3}C^{JM}_{2m_1,2m_2}\psi_{m_1}\psi_{m_2}\psi_{m_3},\\
&\Phi_{30} = -\sqrt{\frac{35}{2}}\sum_{J=0}^{4}\sum_{M=-J}^{J}\sum_{m_1,m_2,m_3=-2}^{2}\\
&\qquad\times C^{00}_{JM,2m_3}C^{JM}_{2m_1,2m_2}\psi_{m_1}\psi_{m_2}\varphi^*_{m_3},\\
&\Gamma_4 = \mathrm{Re}\big[\Psi_{20}\Phi^{*2}_{30}\big].
\end{aligned}
\tag{3}
$$

The GL coefficients can be obtained in the weak coupling limit within the quasiclassical approximation starting from the nonrelativistic spin-1/2 fermion field theory as [56]

$$
\begin{aligned}
K_0 &= \frac{7\zeta(3)N(0)p_{\rm F}^4}{240\pi^2 m_{\rm n}^2T^2}, \qquad \alpha = \frac{N(0)p_{\rm F}^2}{3}\log\frac{T}{T_{\rm c}},\\
\beta_0 &= \frac{7\zeta(3)N(0)p_{\rm F}^4}{60\pi^2T^2}, \qquad \gamma_0 = \frac{31\zeta(5)N(0)p_{\rm F}^6}{13440\pi^4T^4},\\
\delta_0 &= \frac{127\zeta(7)N(0)p_{\rm F}^8}{387072\pi^6T^6}, \quad \beta_2 = \frac{7\zeta(3)N(0)p_{\rm F}^2\gamma_{\rm n}^2}{48(1+F_0^a)^2\pi^2T^2},\\
\gamma_2 &= \frac{31\zeta(5)N(0)p_{\rm F}^4\gamma_{\rm n}^2}{3840(1+F_0^a)^2\pi^4T^4},
\end{aligned}
\tag{4}
$$

with the temperature T, the critical temperature $T_{\rm c}$, the neutron mass $m_{\rm n}$, the neutron gyromagnetic ratio $\gamma_{\rm n}$, the Fermi momentum $p_{\rm F}$, the state-number density $N(0) = m_{\rm n}p_{\rm F}/(2\pi)^2$ at the Fermi surface, and the Landau parameter F_0^a.

The spin-2 spinor order parameter is often written by the 3×3 traceless symmetric matrix A given by

$$
\begin{aligned}
[A]_{11} &= \frac{\sqrt{3}}{2}(\psi_2+\psi_{-2}) - \frac{1}{\sqrt{2}}\psi_0,\\
[A]_{12} &= [A]_{21} = \frac{\sqrt{3}i}{2}(\psi_2-\psi_{-2}),\\
[A]_{13} &= [A]_{31} = -\frac{\sqrt{3}}{2}(\psi_1-\psi_{-1}),\\
[A]_{22} &= -\frac{\sqrt{3}}{2}(\psi_2+\psi_{-2}) - \frac{1}{\sqrt{2}}\psi_0,\\
[A]_{23} &= [A]_{32} = -\frac{\sqrt{3}i}{2}(\psi_1+\psi_{-1}),\\
[A]_{33} &= \sqrt{2}\psi_0.
\end{aligned}
\tag{5}
$$

All candidates for uniform ground states were classified in Ref. [58], and characterized by $U(1)\times SO(3)$ invariants $\boldsymbol{S}^2$, $|\Psi_{20}|^2$, and $|\Psi_{30}|^2$. The five characteristic symmetric states are ferromagnetic ($\boldsymbol{S}^2/\rho^2 = 4\rho^2$, $|\Psi_{20}|^2 = |\Psi_{30}|^2 = 0$), uniaxial nematic (UN) ($\boldsymbol{S}^2 = 0$, $|\Psi_{20}|^2 = \rho^2$, $|\Psi_{30}|^2 = \rho^3$), D_4 biaxial nematic (BN) ($\boldsymbol{S}^2 = 0$, $|\Psi_{20}|^2 = \rho^2$, $|\Psi_{30}|^2 = 0$), D_2 BN ($\boldsymbol{S}^2 = 0$, $|\Psi_{20}|^2 = \rho^2$, $0 < |\Psi_{30}|^2 < \rho^3$), and cyclic ($\boldsymbol{S}^2 = 0$, $|\Psi_{20}|^2 = 0$, $|\Psi_{30}|^2 = 2\rho^3$) states.

For the effective Lagrangian density f in Eq. (1), the UN, D_2 BN, and D_4 BN states are predicted to be realized at $|\boldsymbol{B}| = 0$, $0 < |\boldsymbol{B}| < B_{\rm c}$, and $|\boldsymbol{B}| > B_c$, in $^3P_2$ superfluids [44] as shown in Table I(a). The critical magnetic field $B_{\rm c}$ separating the D_2 BN and D_4 BN states depends on the temperature and takes the maximum value $B_{\rm c} = 7.06\times10^{-2}\pi(1+F_0^a)T_{\rm c}/\gamma_{\rm n}$ at $T \simeq 0.854T_{\rm c}$. With an estimation for the critical temperature $T_{\rm c} \approx 0.2$ MeV and the Landau parameter $F_0^a \approx 1$, this critical magnetic field can be estimated as $B_{\rm c} \approx 7.36\times10^{15}$ G. At $T \lesssim 0.796T_{\rm c}$, we obtain $B_{\rm c} = 0$.

III. VORTEX SOLUTIONS

A. Ansatz

Next, we consider vortex solutions with vortex cores placed at $r = 0$ in the cylindrical coordinate (r, θ, z) and the boundary $\psi|_{r\to\infty}$ far from vortex cores. The vortices and the angular momentum are parallel to the z axis. For the so-called integer vortices, the order parameters behave as $\psi_{-2\leqslant m\leqslant 2}|_{r\to\infty} \propto e^{i\theta}$ around which the overall phase of ψ winds by 2π. In this section, we determine the boundary conditions around the vortices for the cases of $\boldsymbol{B} = 0$ and $\boldsymbol{B} \neq 0$,

For $\boldsymbol{B} = 0$, the uniform ground state is degenerate within the possible UN state

$$
\begin{aligned}
\tilde{\psi}_{\pm2} &= \frac{e^{i(\phi\mp2a)}\sqrt{3}\sin^2 b}{2\sqrt{2}}, \quad \tilde{\psi}_{\pm1} = \mp\frac{e^{i(\phi\mp a)}\sin(2b)}{2\sqrt{2}},\\
\tilde{\psi}_0 &= \frac{e^{i\phi}\{1+3\cos(2b)\}}{4},
\end{aligned}
\tag{6}
$$

or

$$
\begin{aligned}
\tilde{A} &= \frac{1}{\sqrt{2}}R_z^aR_y^b\begin{pmatrix}-1&0&0\\0&-1&0\\0&0&2\end{pmatrix}R_y^{-b}R_z^{-a},\\
R_y^b &\equiv \begin{pmatrix}\cos b&0&\sin b\\0&1&0\\-\sin b&0&\cos b\end{pmatrix},\\
R_z^a &\equiv \begin{pmatrix}\cos a&-\sin a&0\\\sin a&\cos a&0\\0&0&1\end{pmatrix},
\end{aligned}
\tag{7}
$$

for $0 \leqslant a, 2b, \phi \leqslant 2\pi$. Here $\tilde{\psi}$ is defined as $\tilde{\psi} \equiv \psi/\sqrt{\rho}$, and $\tilde{A}$ is defined by replacing A and ψ with $\tilde{A}$ and $\tilde{\psi}$, respectively, in Eq. (5). a, b, and ϕ represent overall spin rotations along z axis and y axis, and overall phase shift, respectively. Under the spatial phase gradient $e^{i\theta}$ for the vortex solution, however, the current-spin-dependent free energy density $f_{202}^{(2)}$ in Eq. (1) favors $b = 0$, giving

$$
\tilde{\psi} \xrightarrow{r\to\infty} (0, 0, e^{i\theta}, 0, 0)^T, \tag{8}
$$

or

$$
\tilde{A} \xrightarrow{r\to\infty} \frac{e^{i\theta}}{\sqrt{2}}\begin{pmatrix}-1&0&0\\0&-1&0\\0&0&2\end{pmatrix}, \tag{9}
$$

We next consider the case of $|\boldsymbol{B}| > 0$. In this paper, the simplest situation $\boldsymbol{B} \parallel \boldsymbol{z}$ is considered, i.e., the magnetic field is parallel to the angular momentum for the vortex. For $0 < |\boldsymbol{B}| < B_c$, field-dependent free energy density $\beta_2 f_{022} + \gamma_2 f_{024}$ favors $\psi_{\pm 2}$, leading

$$\tilde{\psi} \xrightarrow{r\to\infty} e^{i\theta}\left(\frac{e^{-2ia}\sin g}{\sqrt{2}}, 0, \cos g, 0, \frac{e^{2ia}\sin g}{\sqrt{2}}\right)^T, \tag{10}$$

or

$$\tilde{A} \xrightarrow{r\to\infty} \sqrt{2}e^{i\theta}R_z^a\begin{pmatrix}\sin g_- & 0 & 0\\ 0 & -\sin g_+ & 0\\ 0 & 0 & \cos g\end{pmatrix}R_z^{-a}, \tag{11}$$

$$g_\pm \equiv g \pm \frac{\pi}{6},$$

where g depends on $|\boldsymbol{B}|$ and satisfies $\pi/3 < g < \pi/2$, making $\psi|_{r\to\infty}$ to be the D_2 BN state. a also represents the overall spin rotation along z axis as well as that in Eq. (6). Without current-spin-dependent free energy $f_{202}^{(1)}$, a takes the arbitrary value, but is fixed with the finite $f_{202}^{(1)}$ to minimize this. In the limit of $|\boldsymbol{B}| \searrow 0$, g becomes $g \to \pi/3$ giving

$$\tilde{\psi} \xrightarrow{r\to\infty} e^{i\theta}\left(\frac{e^{-2ia}\sqrt{3}}{2\sqrt{2}}, 0, \frac{1}{2}, 0, \frac{e^{2ia}\sqrt{3}}{2\sqrt{2}}\right)^T, \tag{12}$$

or

$$\tilde{A} \xrightarrow{r\to\infty} \frac{e^{i\theta}}{\sqrt{2}}R_z^a\begin{pmatrix}1 & 0 & 0\\ 0 & -2 & 0\\ 0 & 0 & 1\end{pmatrix}R_z^{-a}. \tag{13}$$

This solution belongs to the uniaxial nematic state in Eq. (6) with $b = \pi/2$, but is different from that for $\boldsymbol{B} = 0$ shown in Eq. (8), which leads the discontinuity between $\boldsymbol{B} = 0$ and $|\boldsymbol{B}| \searrow 0$.

In the limit of $|\boldsymbol{B}| \nearrow B_c$, g becomes $g \to \pi/2$, giving

$$\tilde{\psi} \xrightarrow{r\to\infty} e^{i\theta}\left(\frac{e^{-2ia}}{\sqrt{2}}, 0, 0, 0, \frac{e^{2ia}}{\sqrt{2}}\right)^T, \tag{14}$$

or

$$\tilde{A} \xrightarrow{r\to\infty} \sqrt{\frac{3}{2}}e^{i\theta}R_z^a\begin{pmatrix}1 & 0 & 0\\ 0 & -1 & 0\\ 0 & 0 & 0\end{pmatrix}R_z^{-a}. \tag{15}$$

which belongs to the D_4 BN state. For $|\boldsymbol{B}| \geqslant B_c$, the vortex state is the same as that in Eq. (14) that belongs to D_4 BN state.

For the half-quantized vortex, the overall phase of ψ winds by π. To keep the single-valued property of the order parameter, the spin also rotates. Only the D_4 BN state under $|\boldsymbol{B}| > B_c$ enables the half-quantized vortex with the order parameter giving

$$\tilde{\psi} \xrightarrow{r\to\infty} \left(\frac{e^{-2ia}}{\sqrt{2}}, 0, 0, 0, \frac{e^{i(\theta+2a)}}{\sqrt{2}}\right)^T, \tag{16}$$

or

$$\tilde{A} \xrightarrow{r\to\infty} \frac{\sqrt{3}}{2\sqrt{2}}R_z^a\begin{pmatrix}\theta_+ & i\theta_- & 0\\ i\theta_- & -\theta_+ & 0\\ 0 & 0 & 0\end{pmatrix}R_z^{-a}, \tag{17}$$

$$\theta_\pm \equiv e^{i\theta} \pm 1$$

in the case of $\boldsymbol{B} \parallel \boldsymbol{z}$. For the vortex solution (16), the z component of the spin rotates by $\pi/2$ around the vortex. The other solution with the spin rotation by $-\pi/2$ is

$$\tilde{\psi} \xrightarrow{r\to\infty} \left(\frac{e^{i(\theta-2a)}}{\sqrt{2}}, 0, 0, 0, \frac{e^{2ia}}{\sqrt{2}}\right)^T, \tag{18}$$

or

$$\tilde{A} \xrightarrow{r\to\infty} \frac{\sqrt{3}}{2\sqrt{2}}R_z^a\begin{pmatrix}\theta_+ & -i\theta_- & 0\\ -i\theta_- & -\theta_+ & 0\\ 0 & 0 & 0\end{pmatrix}R_z^{-a}. \tag{19}$$

B. Numerical results

In this section, we show the numerical results for the overall vortex state by minimizing the free energy f under the boundary condition

$$\psi_m(\theta + \pi/2) = i\psi_m(\theta), \tag{20}$$

or

$$[A]_{ij}(\theta + \pi/2) = i[A]_{ij}(\theta), \tag{21}$$

at the boundary $r = L/2$, which induces the integer vortex solution. The minimization of the free energy density f can be done by finding the solution of the stationary solution of the GL equation

$$\frac{\delta f}{\delta \psi_m^*} = 0. \tag{22}$$

The solution of Eq. (22) can be obtained by introducing the relaxation time t and the dependence of the order parameter ψ_m on t, and solving

$$\dot{\psi}_m = -\frac{\delta f}{\delta \psi_m^*}. \tag{23}$$

After the long time evolution of Eq. (23), we attain the solution of Eq. (22). With an appropriate scaling of the time t, Eq. (23) is nothing but the time-dependent GL equation that is often used in the research field of superconductivity. However, it has not yet derived from the microscopic theory for the $^3P_2$ superfluids.

Here, L is the system size fixed to be $L = 128p_F/[\pi^2 N(0)T_c^2]$. The temperature is fixed to be $T = 0.854T_c \approx 0.171$ MeV for which B_c takes the maximal value $B_c = 7.06\times10^{-2}\pi(1 + F_0^a)T_c/\gamma_n \approx 7.36\times10^{15}$ G with the critical temperature $T_c \approx 0.2$ MeV and Landau parameter $F_0^a \approx 1$. The magnetic field $\boldsymbol{B}(\parallel \boldsymbol{z})$ changes from 0 to $1.5B_c$.

1. Vortex state with ferromagnetic core in the UN phase

We start from the case of the UN phase at zero magnetic field. Figure 1 shows the squared modulus $|\psi_m|^2$, argument Arg$[\psi_m]$ of the order parameter, $U(1)\times SO(3)$ invariants $\boldsymbol{S}^2$, $|\Psi_{20}|^2$, and $|\Psi_{30}|^2$, and the free energy density f at the

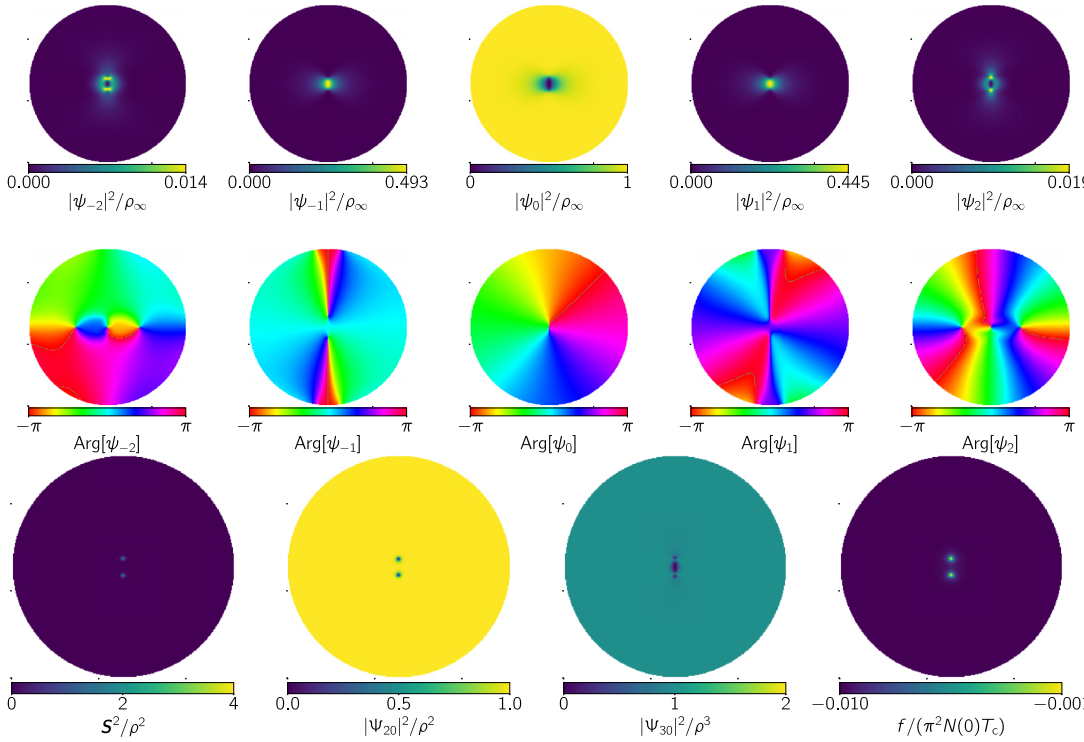

FIG. 1. The vortex state in the UN phase at the zero magnetic field $\boldsymbol{B} = 0$. The squared modulus $|\psi_m|^2$ (top row), argument $\mathrm{Arg}[\psi_m]$ (middle row) of the order parameter, the $U(1)\times SO(3)$ invariants S^2, $|\Psi_{20}|^2$, and $|\Psi_{30}|^2$, and the free energy density f (bottom row) are shown. The radius of the figure shown here is $64 p_{\mathrm{F}}/(\pi m_{\mathrm{n}} T_{\mathrm{c}}) \approx 1.33\times 10^4$ fm. The two half-quantized vortices are connected by a single line soliton of the D_4 BN order.

zero magnetic field $\boldsymbol{B} = 0$. The radius of circles in figures is fixed to be $64\hbar^2 k_{\mathrm{F}}/(\pi M_{\mathrm{n}}^* T_{\mathrm{c}}) \approx 1.33\times 10^4$ fm. Where $k_{\mathrm{F}} = (3\pi^2 n)^{1/3} \approx 2.20$ fm^{-1} is the neutron Fermi wave number with the neutron number density $n \approx 2.25 n_0 \approx 0.36$ fm^{-3} for the saturation density $n_0 \approx 0.16$ fm^{-3} of nuclear matter. M_{n}^* is the effective neutron mass $M_{\mathrm{n}}^* c^2 \approx 0.7 M_{\mathrm{n}} c^2 \approx 658$ MeV for the neutron vacuum mass $M_{\mathrm{n}} c^2 \approx 940$ MeV. The critical temperature is set to be $T_{\mathrm{c}} \approx 0.2$ MeV. The order parameter ψ satisfies Eq. (8) near the edge of the system, where the state belongs to the uniaxial nematic state $S^2 = 0$, $|\Psi_{20}|^2/\rho^2 = |\psi_{30}|^2/\rho^3 = 1$. At the center of the system, there are two holes of $|\Psi_{20}|^2$ implying the breakdown of the UN order. These two holes correspond to the vortex cores and each of them carries half-circulations. This result clearly shows that a singly quantized vortex splits into two half-quantized non-Abelian vortices around the vortex core. The fact that isolated half-quantized vortices can topologically exist only in the D_4 BN state implies that the D_4 BN order should appear around the vortex core. In fact, we can confirm that the D_4 BN order characterized by $S^2 = 0$, $|\Psi_{20}|^2/\rho^2 = 1$, and $|\Psi_{30}|^2/\rho^3 = 0$ appears along a line structure bridging two vortex cores, as can be seen in the plot of $|\Psi_{30}|^2$ locally inducing the D_4 BN order and half-quantized vortices. On the other hand, at the vortex cores, the $U(1)\times SO(3)$ invariants are $S^2/\rho^2 \simeq 4$ and $|\Psi_{20}|^2/\rho^2 = |\psi_{30}|^2/\rho^3 = 0$, implying the appearance of the ferromagnetic order. Therefore, we characterize this vortex by the ferromagnetic core. In this phase, there is also a metastable vortex molecule state with the cyclic cores similar to the D_2 phase discussed below.

2. *Vortex state with the cyclic core in the D_2 BN phase*

At $|\boldsymbol{B}| = 0.5 B_{\mathrm{c}}$ as shown in Fig. 2, the order parameter drastically changes from that in Eq. (8) to that in Eq. (10) where $\psi_{\pm 2}$ become finite at $r \to \infty$. As well as the case for $\boldsymbol{B} = 0$, a singly quantized vortex splits into two half-quantized vortices with two holes of $|\Psi_{20}|^2$. In contrast to the vortex molecule in the UN phase, there are three soliton lines of D_4 BN order with $|\Psi_{30}|^2/\rho^3 = 0$ bridging two half-quantized vortices. At the vortex cores, we have $S^2/\rho^2 \simeq 0$ and $|\psi_{30}|^2/\rho^3 \simeq 2$ supporting the cyclic order. We characterize this vortex by the cyclic core. With turning off the magnetic field, it becomes a metastable state with higher energy than the lowest-energy state of the vortex molecule discussed in Sec. III B 1.

3. *Vortex state with the cyclic core in the D_4 BN phase*

At $|\boldsymbol{B}| > B_{\mathrm{c}}$, the order parameter in the bulk becomes the D_4 BN state shown in Eq. (14) at $r \to \infty$. Figure 3 shows the $SO(3)$ invariants and the free energy density at the magnetic field $|\boldsymbol{B}| = 1.3 B_{\mathrm{c}}$. Although one half-quantized vortex is topologically stable in this state, two half-quantized vortices form a bound state to be an integer vortex. The cores of half-quantized vortices are filled with the cyclic order having $S^2/\rho^2 \simeq 0$ and $|\psi_{30}|^2/\rho^3 \simeq 2$ as well as the case of

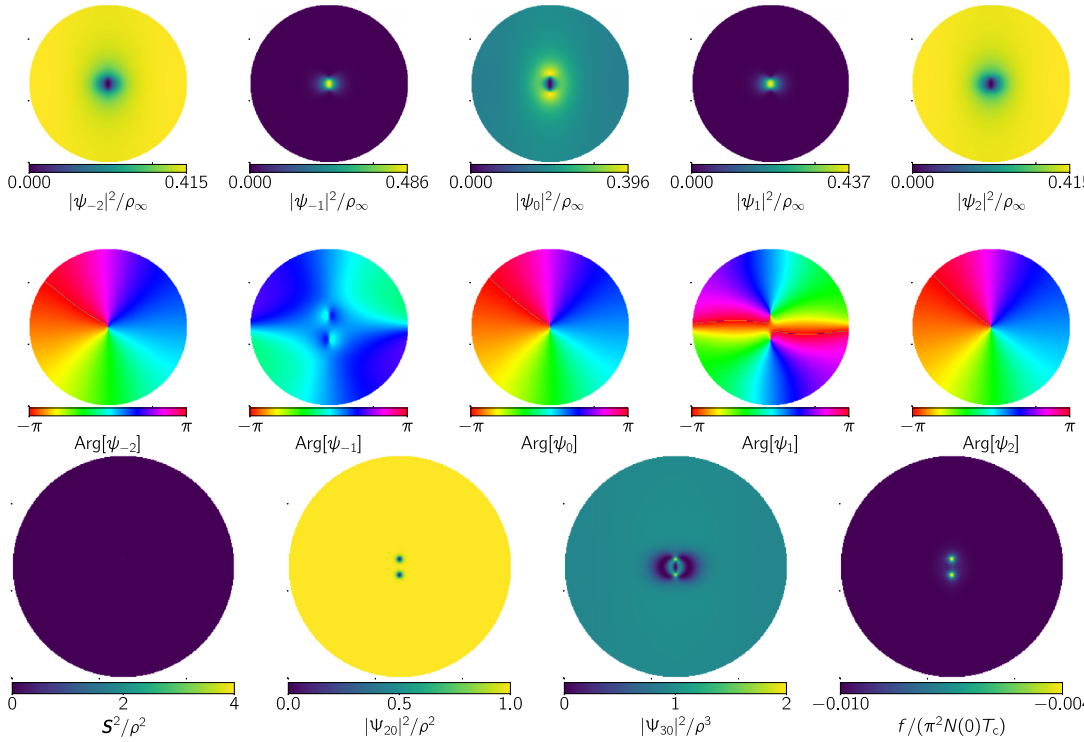

FIG. 2. The vortex state in the D_2 BN phase at the magnetic field $\boldsymbol{B} = 0.5 B_c \hat{z}$. The squared modulus $|\psi_m|^2$ (top row), argument Arg$[\psi_m]$ (middle row) of the order parameter, the $U(1)\times SO(3)$ invariants $\boldsymbol{S}^2$, $|\Psi_{20}|^2$, and $|\Psi_{30}|^2$, and the free energy density f (bottom row) are shown. The radius of the figure shown here is $64 p_F/(\pi m_n T_c) \approx 1.33\times 10^4$ fm. The two half-quantized vortices are connected by three line solitons with the D_4 BN order in their cores.

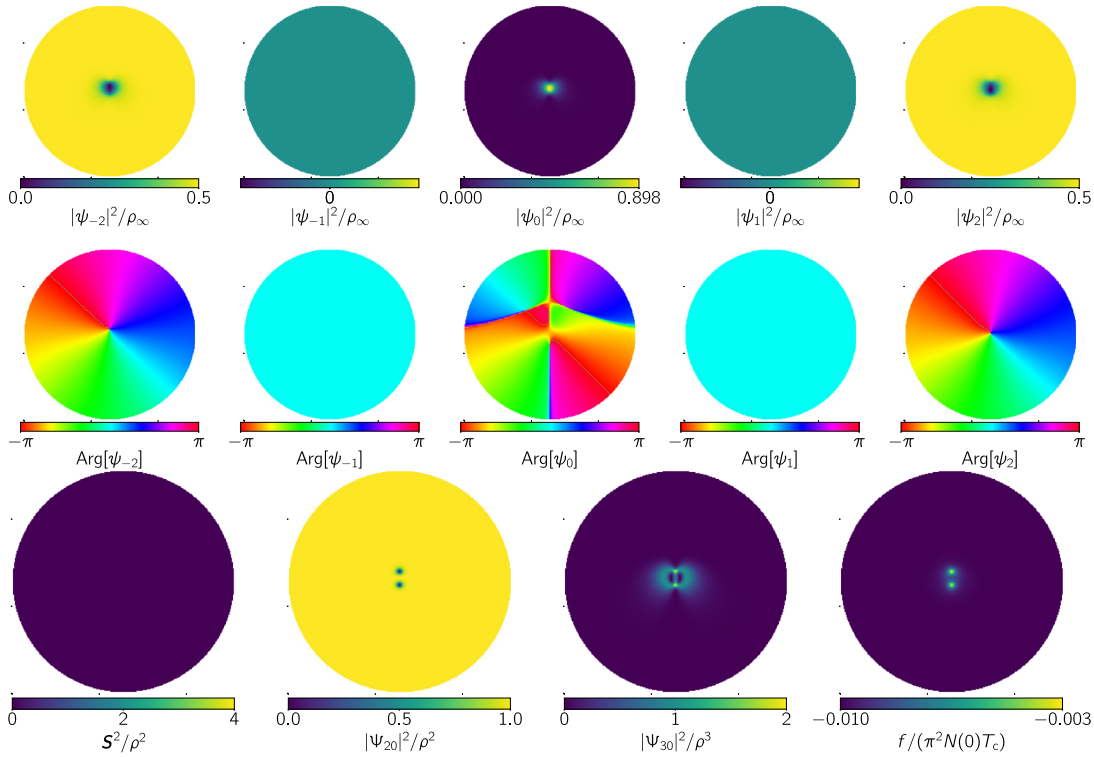

FIG. 3. The vortex state in the D_4 BN phase at the magnetic field $\boldsymbol{B} = 1.3 B_c \hat{z}$. Squared modulus $|\psi_m|^2$ (top row), argument Arg$[\psi_m]$ (middle row) of the order parameter, the $U(1)\times SO(3)$ invariants $\boldsymbol{S}^2$, $|\Psi_{20}|^2$, and $|\Psi_{30}|^2$, and the free energy density f are shown. The radius of the figure shown here is $64 p_F/(\pi m_n T_c) \approx 1.33\times 10^4$ fm. The two half-quantized vortices are connected by three line solitons of the D_2 BN order in their cores.

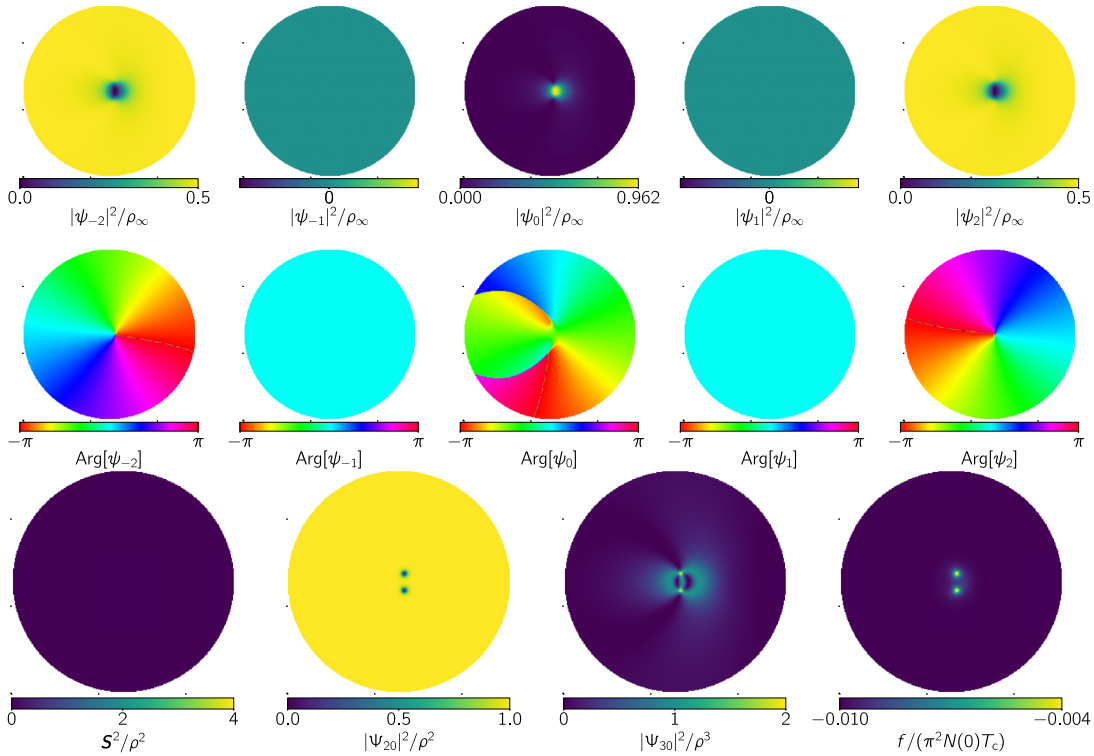

FIG. 4. The vortex state at the boundary between the D_2 BN and D_4 BN phases at the magnetic field $\boldsymbol{B} = B_c\hat{z}$. The squared modulus $|\psi_m|^2$ (top row), argument $\mathrm{Arg}[\psi_m]$ (middle row) of the order parameter, the $U(1)\times SO(3)$ invariants S^2, $|\Psi_{20}|^2$, and $|\Psi_{30}|^2$, and the free energy density f are shown. The radius of the figure shown here is $64p_F/(\pi m_n T_c) \approx 1.33\times10^4$ fm. The two half-quantized non-Abelian vortices are connected by three line solitons asymmetrically.

the D_2 BN phase ($0 < |\boldsymbol{B}| < B_c$). In contrast to the case of the D_2 BN phase, the three line solitons bridging two half-quantized vortices are characterized by the D_2 BN order with $0 < |\Psi_{30}|^2/\rho^3 < 1$.

Our results suggest that the order of three line solitons connecting the two half-quantized vortices are exchanged between D_2 and D_4 BN orders for $|\boldsymbol{B}| < B_c$ and $|\boldsymbol{B}| > B_c$, respectively. Another characteristic feature of the case of $|\boldsymbol{B}| > B_c$ is a fact that $\psi_{\pm1}$ components completely vanish.

4. Vortex state at the boundary between the D_2 and D_4 BN phases

Figure 4 shows the vortex state at the critical magnetic field $|\boldsymbol{B}| = B_c$. Especially, we can see the asymmetric shape of $|\Psi_{30}|^2/\rho^3$ as an intermediate state between those below and above the critical magnetic field B_c, in which two D_4 and D_2 BN orders compete as candidates of the line solitons connecting the two half-quantized vortices. This asymmetric structure of the vortex core soon vanishes as the magnetic field $\boldsymbol{B}$ becomes away from the critical magnetic field B_c. In our case, the vortex core becomes symmetric at $|\boldsymbol{B}| = 0.9B_c$ and $|\boldsymbol{B}| = 1.1B_c$.

5. Energetics and distance between half-quantized vortices

Figure 5(a) shows the free energy $F = \int dr d\theta\, rf$ as a function of the magnetic field $|\boldsymbol{B}|$. The free energy F monotonically increases with magnetic field, and it is continuous when the magnetic field across the critical one B_c. At the zero magnetic field $\boldsymbol{B} = 0$, the vortex solution with ferromagnetic cores with the boundary condition in Eq. (8) has the lower free energy F than that with the cyclic cores and the boundary shown in Eq. (10), and discontinuously connects at $\boldsymbol{B} = 0$. However, a vortex solution with cyclic cores with the boundary in Eq. (10) can also exist as the metastable solution, continuously connecting to the solutions in the D_2 BN phase $|\boldsymbol{B}| > 0$.

Figure 5(b) shows the distance Δ between two half-quantized vortices as a function of the magnetic field $|\boldsymbol{B}|$. Δ monotonically decreases with the magnetic field $|\boldsymbol{B}|$, discontinuously increases at $|\boldsymbol{B}| = B_c$, and again monotonically decreases for $|\boldsymbol{B}| > B_c$. At the zero magnetic field $\boldsymbol{B} = 0$, the half-quantized vortices having the ferromagnetic cores have smaller Δ than that for those having the cyclic cores.

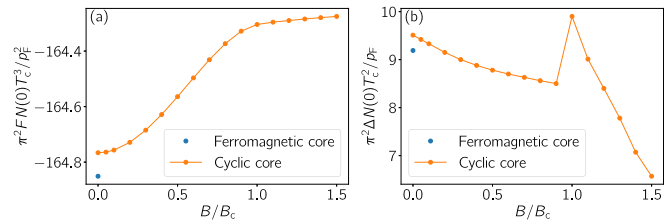

FIG. 5. (a) Free energy F and (b) distance Δ between two half-quantized non-Abelian vortices as a function of the magnetic field $|\boldsymbol{B}|$.

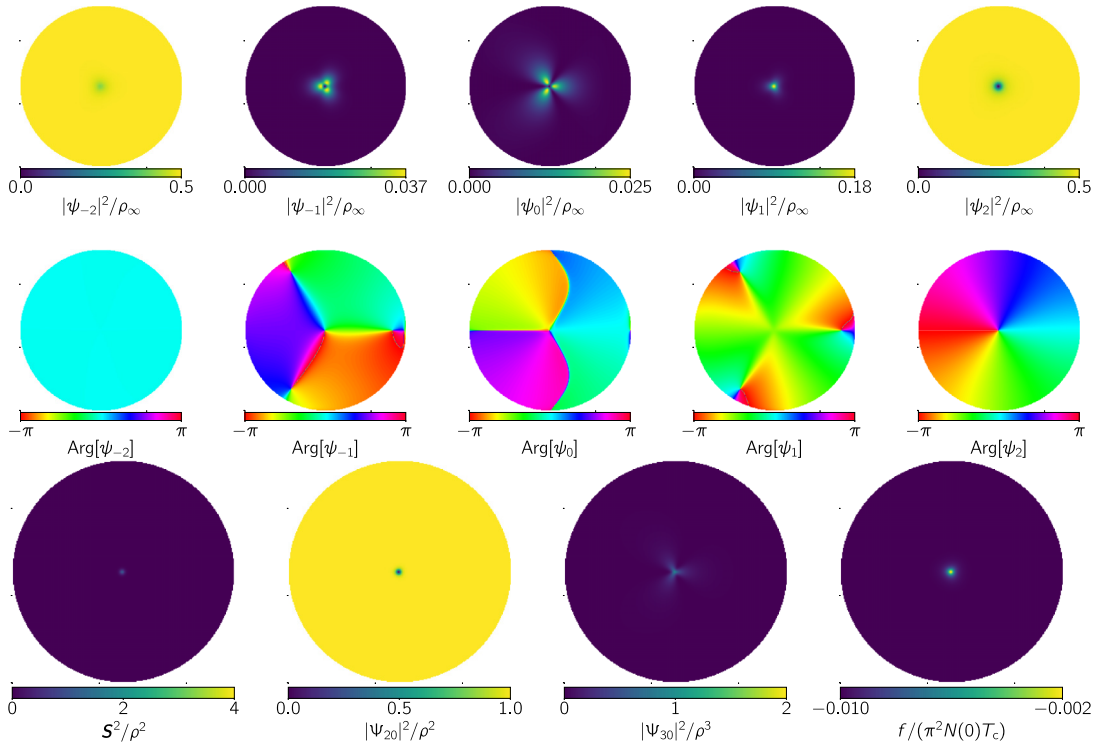

FIG. 6. A single isolated half-quantized non-Abelian vortex in the D_4 BN phase at the magnetic field $\boldsymbol{B} = 1.3B_c\hat{z}$. The squared modulus $|\psi_m|^2$ (top row), argument $\mathrm{Arg}[\psi_m]$ (middle row) of the order parameter, the $U(1)\times SO(3)$ invariants $\boldsymbol{S}^2$, $|\Psi_{20}|^2$, and $|\Psi_{30}|^2$, and the free energy density f are shown. The radius of the figure shown here is $64p_F/(\pi m_n T_c) \approx 1.33\times 10^4$ fm.

6. Isolated half-quantized vortices in the D_4 BN phase

Finally, we also obtain the solution for a single half-quantized vortex at $|\boldsymbol{B}| > B_c$. We put the boundary condition as

$$\begin{aligned} &\psi_2(\theta+\pi/2) = i\psi_2(\theta), \\ &\psi_{1,0,-1} = 0, \\ &\psi_{-2}(\theta+\pi) = \psi_{-2}(\theta), \end{aligned} \tag{24}$$

or

$$\begin{aligned} [A]_{11}(\theta+\pi/2) &= -[A]_{22}(\theta+\pi/2) \\ &= \frac{e^{i\pi/4}}{\sqrt{2}}\{[A]_{11}(\theta) - [A]_{12}(\theta)\}, \\ [A]_{12}(\theta+\pi/2) &= [A]_{21}(\theta+\pi/2) \\ &= \frac{e^{i\pi/4}}{\sqrt{2}}\{[A]_{11}(\theta) + [A]_{12}(\theta)\}, \\ [A]_{13} &= [A]_{23} = [A]_{31} = [A]_{32} = [A]_{33} = 0 \end{aligned} \tag{25}$$

at the boundary which induces half-quantized vortex solutions. Figure 6 shows a single half-quantized vortex state at $|\boldsymbol{B}| = 1.3B_c$. The system has a threefold rotational symmetry around the vortex core, which can be seen in $|\psi_{-1}|^2$, $|\psi_0|^2$, and $|\Psi_{30}|^2$. The existence of the threefold symmetry in $|\Psi_{30}|^2$ is closely related to the existence of the three soliton lines between two half-quantized vortices for the vortex shown in Fig. 3. Such a threefold symmetry at the vortex core has been also observed in ultracold spin-2 atomic BECs [125].

One of the main differences of the isolated half-quantized vortex in Fig. 6 from the constituent one in the molecule in Fig. 3 is that the vortex core in Fig. 6 is filled with the state having $\boldsymbol{S}^2/\rho^2 > 0$ and $|\Psi_{30}|^2/\rho^3 > 0$, which corresponds to the mixed state [58] being intermediate state between the ferromagnetic and cyclic states. Another difference is that $\psi_{\pm 1}$ takes finite values near the vortex core.

IV. SUMMARY AND DISCUSSION

In this paper, we have presented vortex solutions, that is, singly quantized vortices and half-quantized non-Abelian vortices, in the neutron $^3P_2$ superfluids in the case that the external magnetic field is parallel to the angular momentum of the vortices. We have found that a singly quantized vortex splits into two half-quantized non-Abelian vortices connected by soliton(s) forming a vortex molecule, at any strength of the magnetic field. The main results are summarized in Table I. In the absence of the magnetic field in which the UN state is the bulk ground state, the cores of the half-quantized vortices are filled with the ferromagnetic states, and a single linear soliton with the D_4 BN state connects the two half-quantized vortices, as shown in Fig. 1. At the finite magnetic field below the critical one separating D_2 and D_4 BN states, the bulk ground state is the D_2 BN state. In this case, the cores of the half-quantized vortices are filled with the cyclic state and are connected by three line solitons composed of the D_4 BN order, as shown in Fig. 2. Above the critical magnetic field for which the bulk ground state is the D_4 BN state, a single half-quantized vortex is topologically allowed stably, as constructed in Fig. 6.

Nevertheless, two half-quantized vortices are confined with three line solitons composed of D_2 BN order, still forming a vortex molecule as shown in Fig. 3. At the critical magnetic field, the vortex core becomes asymmetric as in Fig. 4, as an intermediate state between the two kinds of molecules of two half-quantized vortices connected by the three D_4 BN solitons and those connected by the three D_2 BN solitons. We have also found that the energy of the vortex molecule monotonically increases as the magnetic field increases, which is continuous including the critical magnetic field as in Fig. 5(a). The distance between the two half-quantized vortices decreases as the magnetic field increases, except for a discontinuous jump with an increase at the critical magnetic field in Fig. 5(b).

Except for the case of the zero magnetic field, vortex cores are always filled with the cyclic state, which also appears even at the zero magnetic field as a metastable state as in Fig. 5(a). Our results contradict with the BdG approach [79,80,126] in which vortex cores are filled with the mixed state for $|\boldsymbol{B}| < B_{\rm c}$ [126] without $\psi_{\pm 1}$ components and completely separated as two isolated half-quantized vortices without linear soliton [80] for $|\boldsymbol{B}| > B_{\rm c}$. A main possible reason for this contradiction comes from the difference of the GL and BdG approaches. The latter approach has an advantage in describing the microscopic structure such as vortex cores and fermion degrees of freedom, and the cyclic state inside cores that we have obtained could be an artifact of the low-energy theory. We should study this point in more detail with, for example, a GL expansion to higher order. Another minor possible reason is the difference of treatments of the boundary condition and positions of half-quantized vortices. In the previous study, the boundary is fixed with the bulk integer vortex state [Eqs. (10) and (14)]. The positions of the half-quantized vortices are also fixed and treated as a differential parameter. On the other hand, neither boundary state determined in the boundary condition (20) nor the positions of half-quantized vortices are fixed and automatically determined to minimize the whole free energy density in our study. This subtle difference may affect the difference of the vortex-core states.

Here we address further discussions for future studies. We here have studied only the case for the magnetic field parallel to the angular momentum (the direction of vortices). We will report the case for an arbitrary angle between them elsewhere, which should be important for study of neutron stars in more general situations.

Further studies should be done for multiple vortex states such as a vortex lattice under rapid rotation relevant for neutron star interiors. In particular, it is important to study whether, in a vortex lattice, constituent half-quantized vortices are still tightly bound as a singly quantized vortex as found in this paper or they are separated by distances of the same order as two-component BECs [108,109,114] and whether a lattice is triangular or square.

Another important subject is a collision dynamics of vortices in three spatial dimensions. It is important whether two vortices reconnect in collision or a formation of a rung between them occurs as the case of non-Abelian vortices in the cyclic phase of spin-2 spinor BECs [127]. The presence or absence of such a vortex reconnection is crucial for states of the quantum turbulence. With this regards, vortex reconnection was reported in the nematic phase of a spin-2 BEC [86], a superfluid similar to $^3P_2$ superfluids. Collision of two vortex molecules may be accompanied by swapping partners as found in vortex molecules in two-component BECs [120].

The coexistence of $^1S_0$ and $^3P_2$ superfluids drastically changes the phase diagram [128], and vortex states in this case will be also one direction to be explored. In this case, vortices having winding only in either of $^1S_0$ and $^3P_2$ condensates would be further fractionalized. In addition, vortex states in the ferromagnetic phase appearing without quasiclassical approximation in the region close to the critical temperature [59] are also interesting to be investigated.

Recently, it has been proposed that in the deep inside of neutron star cores, the quark-hadron continuity for two-flavor quarks holds; the $^3P_2$ superfluid (nuclear matter) is continuously connected through crossover to a two-flavor quark matter called the 2SC+dd phase [129]; in addition to the conventional 2SC phase, a P-wave condensation $\langle d\nabla d\rangle$ is suggested. Vortex structures in the 2SC+dd phase were studied in Refs. [130–132] in which an exotic vortex called a non-Abelian Alice string was found. In particular, in Ref. [131], how vortices in nuclear and quark matter should be connected along the crossover. It will be interesting whether core structures found in this paper are preserved or deformed along this connection. Finally, a novel type of the Berezinskii-Kosterlitz-Thouless (BKT) transition of vortex molecules in two-component systems was reported in Ref. [121], and thus the BKT transition should be investigated in neutron $^3P_2$ superfluids.

ACKNOWLEDGMENTS

We would like to thank Yusuke Masaki for helpful discussions and comments. The work of M.K. is partly supported by JSPS KAKENHI (Grants No. 20K03765, No. 19KK0066), and by Osaka City University Advanced Mathematical Institute (MEXT Joint Usage/Research Center on Mathematics and Theoretical Physics JPMXP0619217849). The work of M.N. is supported in part by JSPS KAKENHI (Grant No. JP18H01217).

[1] V. Graber, N. Andersson, and M. Hogg, Int. J. Mod. Phys. D **26**, 1730015 (2017).

[2] G. Baym, T. Hatsuda, T. Kojo, P. D. Powell, Y. Song, and T. Takatsuka, Rep. Prog. Phys. **81**, 056902 (2018).

[3] P. Demorest, T. Pennucci, S. Ransom, M. Roberts, and J. Hessels, Nature (London) **467**, 1081 (2010).

[4] J. Antoniadis, P. C. C. Freire, N. Wex, T. M. Tauris, R. S. Lynch, M. H. van Kerkwijk, M. Kramer, C. Bassa, V. S. Dhillon, T. Driebe, J. W. T. Hessels, V. M. Kaspi, V. I. Kondratiev, N. Langer, T. R. Marsh, M. A. McLaughlin, T. T. Pennucci, S. M. Ransom, I. H. Stairs, J. van Leeuwen *et al.*, Science **340**, 1233232 (2013).

[5] B. Abbott *et al.* (Virgo, LIGO Scientific), Phys. Rev. Lett. **119**, 161101 (2017).
[6] B. P. Abbott Jr. *et al.* (LIGO Scientific, Virgo), Astrophys. J. Lett. **892**, L3 (2020).
[7] T. E. Riley *et al.*, Astrophys. J. Lett. **887**, L21 (2019).
[8] M. Miller *et al.*, Astrophys. J. Lett. **887**, L24 (2019).
[9] A. B. Migdal, Zh. Eksp. Teor. Fiz. **37**, 249 (1959) [Sov. Phys. JETP **10**, 176 (1960)].
[10] N. Chamel and P. Haensel, Living Rev. Relativ. **11**, 10 (2008).
[11] N. Chamel, J. Astrophys. Astron. **38**, 43 (2017).
[12] B. Haskell and A. Sedrakian, Astrophys. Space Sci. Libr. **457**, 401 (2018).
[13] A. Sedrakian and J. W. Clark, Eur. Phys. J. A **55**, 167 (2019).
[14] N. Andersson, Universe **7**, 17 (2021).
[15] G. Baym, C. Pethick, D. Pines, and M. Ruderman, Nature (London) **224**, 872 (1969).
[16] D. Pines, J. Shaham, and M. Ruderman, Nat. Phys. Sci. **237**, 83 (1972).
[17] T. Takatsuka and R. Tamagaki, Prog. Theor. Phys. **79**, 274 (1988).
[18] D. G. Yakovlev, A. D. Kaminker, O. Y. Gnedin, and P. Haensel, Phys. Rep. **354**, 1 (2001).
[19] A. Y. Potekhin, J. A. Pons, and D. Page, Space Sci. Rev. **191**, 239 (2015).
[20] D. G. Yakovlev, K. P. Levenfish, and Yu. A. Shibanov, Phys.-Usp. **42**, 737 (1999).
[21] C. O. Heinke and W. C. G. Ho, Astrophys. J. **719**, L167 (2010).
[22] P. S. Shternin, D. G. Yakovlev, C. O. Heinke, W. C. G. Ho, and D. J. Patnaude, Mon. Not. Roy. Astron. Soc. Lett. **412**, L108 (2011).
[23] D. Page, M. Prakash, J. M. Lattimer, and A. W. Steiner, Phys. Rev. Lett. **106**, 081101 (2011).
[24] R. A. Wolf, Astrophys. J. **145**, 834 (1966).
[25] F. Tabakin, Phys. Rev. **174**, 1208 (1968).
[26] M. Hoffberg, A. E. Glassgold, R. W. Richardson, and M. Ruderman, Phys. Rev. Lett. **24**, 775 (1970).
[27] R. Tamagaki, Prog. Theor. Phys. **44**, 905 (1970).
[28] T. Takatsuka and R. Tamagaki, Prog. Theor. Phys. **46**, 114 (1971).
[29] T. Takatsuka, Prog. Theor. Phys. **47**, 1062 (1972).
[30] T. Fujita and T. Tsuneto, Prog. Theor. Phys. **48**, 766 (1972).
[31] R. W. Richardson, Phys. Rev. D **5**, 1883 (1972).
[32] L. Amundsen and E. Ostgaard, Nucl. Phys. A **442**, 163 (1985).
[33] T. Takatsuka and R. Tamagaki, Prog. Theor. Phys. Suppl. **112**, 27 (1993).
[34] M. Baldo, J. Cugnon, A. Lejeune, and U. Lombardo, Nucl. Phys. A **536**, 349 (1992).
[35] Ø. Elgarøy, L. Engvik, M. Hjorth-Jensen, and E. Osnes, Nucl. Phys. A **607**, 425 (1996).
[36] V. A. Khodel, V. V. Khodel, and J. W. Clark, Phys. Rev. Lett. **81**, 3828 (1998).
[37] M. Baldo, O. Elgaroy, L. Engvik, M. Hjorth-Jensen, and H. J. Schulze, Phys. Rev. C **58**, 1921 (1998).
[38] V. V. Khodel, V. A. Khodel, and J. W. Clark, Nucl. Phys. A **679**, 827 (2001).
[39] M. V. Zverev, J. W. Clark, and V. A. Khodel, Nucl. Phys. A **720**, 20 (2003).
[40] S. Maurizio, J. W. Holt, and P. Finelli, Phys. Rev. C **90**, 044003 (2014).
[41] S. K. Bogner, R. J. Furnstahl, and A. Schwenk, Prog. Part. Nucl. Phys. **65**, 94 (2010).
[42] S. Srinivas and S. Ramanan, Phys. Rev. C **94**, 064303 (2016).
[43] M. Stein, A. Sedrakian, X.-G. Huang, and J. W. Clark, Phys. Rev. C **93**, 015802 (2016).
[44] T. Mizushima, K. Masuda, and M. Nitta, Phys. Rev. B **95**, 140503(R) (2017).
[45] A. P. Schnyder, S. Ryu, A. Furusaki, and A. W. W. Ludwig, Phys. Rev. B **78**, 195125 (2008).
[46] S. Ryu, A. P. Schnyder, A. Furusaki, and A. W. W. Ludwig, New J. Phys. **12**, 065010 (2010).
[47] N. D. Mermin, Phys. Rev. A **9**, 868 (1974).
[48] J. A. Sauls and J. W. Serene, Phys. Rev. D **17**, 1524 (1978).
[49] P. Muzikar, J. A. Sauls, and J. W. Serene, Phys. Rev. D **21**, 1494 (1980).
[50] J. A. Sauls, D. L. Stein, and J. W. Serene, Phys. Rev. D **25**, 967 (1982).
[51] V. Z. Vulovic and J. A. Sauls, Phys. Rev. D **29**, 2705 (1984).
[52] K. Masuda and M. Nitta, Phys. Rev. C **93**, 035804 (2016).
[53] K. Masuda and M. Nitta, Prog. Theor. Exp. Phys. **2020**, 013 (2020).
[54] S. Yasui, C. Chatterjee, and M. Nitta, Phys. Rev. C **99**, 035213 (2019).
[55] S. Yasui, C. Chatterjee, and M. Nitta, JPS Conf. Proc. **26**, 024022 (2019).
[56] S. Yasui, C. Chatterjee, M. Kobayashi, and M. Nitta, Phys. Rev. C **100**, 025204 (2019).
[57] T. Mizushima, S. Yasui, and M. Nitta, Phys. Rev. Res. **2**, 013194 (2020).
[58] M. Kobayashi and M. Nitta, Phys. Rev. A **104**, 053302 (2021).
[59] T. Mizushima, S. Yasui, D. Inotani, and M. Nitta, Phys. Rev. C **104**, 045803 (2021).
[60] P. F. Bedaque, G. Rupak, and M. J. Savage, Phys. Rev. C **68**, 065802 (2003).
[61] L. B. Leinson, Phys. Lett. B **702**, 422 (2011).
[62] L. B. Leinson, Phys. Rev. C **85**, 065502 (2012).
[63] L. B. Leinson, Phys. Rev. C **87**, 025501 (2013).
[64] P. F. Bedaque and A. N. Nicholson, Phys. Rev. C **87**, 055807 (2013); **89**, 029902(E) (2014).
[65] P. Bedaque and S. Sen, Phys. Rev. C **89**, 035808 (2014).
[66] P. F. Bedaque and S. Reddy, Phys. Lett. B **735**, 340 (2014).
[67] P. F. Bedaque, A. N. Nicholson, and S. Sen, Phys. Rev. C **92**, 035809 (2015).
[68] L. B. Leinson, Phys. Rev. C **81**, 025501 (2010).
[69] L. B. Leinson, Phys. Lett. B **689**, 60 (2010).
[70] L. B. Leinson, Phys. Rev. C **82**, 065503 (2010); **84**, 049901(E) (2011).
[71] L. B. Leinson, Phys. Rev. C **83**, 055803 (2011).
[72] L. B. Leinson, Phys. Rev. C **84**, 045501 (2011).
[73] S. Yasui and M. Nitta, Phys. Rev. C **101**, 015207 (2020).
[74] S. Yasui, C. Chatterjee, and M. Nitta, Phys. Rev. C **101**, 025204 (2020).
[75] P. E. Reichley and G. S. Downs, Nature Phys. Sci. **234**, 48 (1971).
[76] P. W. Anderson and N. Itoh, Nature (London) **256**, 25 (1975).
[77] C. Chatterjee, M. Haberichter, and M. Nitta, Phys. Rev. C **96**, 055807 (2017).
[78] L. B. Leinson, Mon. Not. Roy. Astron. Soc. **498**, 304 (2020).
[79] Y. Masaki, T. Mizushima, and M. Nitta, Phys. Rev. Res. **2**, 013193 (2020).

[80] Y. Masaki, T. Mizushima, and M. Nitta, arXiv:2107.02448.
[81] G. Marmorini, S. Yasui, and M. Nitta, arXiv:2010.09032.
[82] F. Zhou and G. W. Semenoff, Phys. Rev. Lett. **97**, 180411 (2006).
[83] G. W. Semenoff and F. Zhou, Phys. Rev. Lett. **98**, 100401 (2007).
[84] S. Uchino, M. Kobayashi, and M. Ueda, Phys. Rev. A **81**, 063632 (2010).
[85] S. Uchino, M. Kobayashi, M. Nitta, and M. Ueda, Phys. Rev. Lett. **105**, 230406 (2010).
[86] M. O. Borgh and J. Ruostekoski, Phys. Rev. Lett. **117**, 275302 (2016); **118**, 129901(E) (2017).
[87] H. Schmaljohann, M. Erhard, J. Kronjäger, M. Kottke, S. van Staa, L. Cacciapuoti, J. J. Arlt, K. Bongs, and K. Sengstock, Phys. Rev. Lett. **92**, 040402 (2004).
[88] M.-S. Chang, C. D. Hamley, M. D. Barrett, J. A. Sauer, K. M. Fortier, W. Zhang, L. You, and M. S. Chapman, Phys. Rev. Lett. **92**, 140403 (2004).
[89] T. Kuwamoto, K. Araki, T. Eno, and T. Hirano, Phys. Rev. A **69**, 063604 (2004).
[90] A. Widera, F. Gerbier, S. Fölling, T. Gericke, O. Mandel, and I. Bloch, New J. Phys. **8**, 152 (2006).
[91] S. Tojo, A. Tomiyama, M. Iwata, T. Kuwamoto, and T. Hirano, Appl. Phys. B **93**, 403 (2008).
[92] S. Tojo, T. Hayashi, T. Tanabe, T. Hirano, Y. Kawaguchi, H. Saito, and M. Ueda, Phys. Rev. A **80**, 042704 (2009).
[93] S. Kobayashi, M. Kobayashi, Y. Kawaguchi, M. Nitta, and M. Ueda, Nucl. Phys. B **856**, 577 (2012).
[94] E. Babaev, Phys. Rev. Lett. **89**, 067001 (2002).
[95] E. Babaev, A. Sudbo, and N. W. Ashcroft, Nature (London) **431**, 666 (2004).
[96] J. Goryo, S. Soma, and H. Matsukawa, Europhys. Lett. **80**, 17002 (2007).
[97] Y. Tanaka, A. Crisan, D. D. Shivagan, A. Iyo, K. Tokiwa, and T. Watanabe, Jpn. J. Appl. Phys. **46**, 134 (2007).
[98] A. Crisan, Y. Tanaka, D. D. Shivagan, A. Iyo, L. Cosereanu, K. Tokiwa, and T. Watanabe, Jpn. J. Appl. Phys. **46**, L451 (2007).
[99] J. W. Guikema, H. Bluhm, D. A. Bonn, R. Liang, W. N. Hardy, and K. A. Moler, Phys. Rev. B **77**, 104515 (2008).
[100] M. Nitta, M. Eto, T. Fujimori, and K. Ohashi, J. Phys. Soc. Jpn. **81**, 084711 (2012).
[101] J. Garaud, J. Carlstrom, and E. Babaev, Phys. Rev. Lett. **107**, 197001 (2011).
[102] J. Garaud, J. Carlström, E. Babaev, and M. Speight, Phys. Rev. B **87**, 014507 (2013).
[103] J. Garaud and E. Babaev, Phys. Rev. B **86**, 060514(R) (2012).
[104] Y. Tanaka, H. Yamamori, T. Yanagisawa, T. Nishio, and S. Arisawa, Physica C **538**, 12 (2017).
[105] Y. Tanaka, H. Yamamori, T. Yanagisawa, T. Nishio, and S. Arisawa, Physica C **548**, 44 (2018).
[106] C. Chatterjee, S. B. Gudnason, and M. Nitta, J. High Energy Phys. 04 (2020) 109.
[107] D. T. Son and M. A. Stephanov, Phys. Rev. A **65**, 063621 (2002).
[108] E. J. Mueller and T.-L. Ho, Phys. Rev. Lett. **88**, 180403 (2002).
[109] K. Kasamatsu, M. Tsubota, and M. Ueda, Phys. Rev. Lett. **91**, 150406 (2003).
[110] K. Kasamatsu, M. Tsubota, and M. Ueda, Phys. Rev. Lett. **93**, 250406 (2004).
[111] P. Kuopanportti, J. A. M. Huhtamäki, and M. Möttönen, Phys. Rev. A **85**, 043613 (2012).
[112] A. Aftalion, P. Mason, and J. Wei, Phys. Rev. A **85**, 033614 (2012).
[113] M. Eto and M. Nitta, Phys. Rev. A **85**, 053645 (2012).
[114] M. Cipriani and M. Nitta, Phys. Rev. Lett. **111**, 170401 (2013).
[115] M. Eto and M. Nitta, Europhys. Lett. **103**, 60006 (2013).
[116] M. Nitta, M. Eto, and M. Cipriani, J. Low Temp. Phys. **175**, 177 (2014).
[117] D. S. Dantas, A. R. P. Lima, A. Chaves, C. A. S. Almeida, G. A. Farias, and M. V. Milošević, Phys. Rev. A **91**, 023630 (2015).
[118] M. Tylutki, L. P. Pitaevskii, A. Recati, and S. Stringari, Phys. Rev. A **93**, 043623 (2016).
[119] M. Eto and M. Nitta, Phys. Rev. A **97**, 023613 (2018).
[120] M. Eto, K. Ikeno, and M. Nitta, Phys. Rev. Res. **2**, 033373 (2020).
[121] M. Kobayashi, M. Eto, and M. Nitta, Phys. Rev. Lett. **123**, 075303 (2019).
[122] B. Mencia Uranga and A. Lamacraft, Phys. Rev. A **97**, 043609 (2018).
[123] M. Eto and M. Nitta, Phys. Rev. D **104**, 094052 (2021).
[124] M. Eto, Y. Hamada, and M. Nitta, J. High Energy Phys. 02 (2022) 099.
[125] M. Kobayashi, Y. Kawaguchi, and M. Ueda, arXiv:0907.3716.
[126] Y. Masaki, T. Mizushima, and M. Nitta (unpublished).
[127] M. Kobayashi, Y. Kawaguchi, M. Nitta, and M. Ueda, Phys. Rev. Lett. **103**, 115301 (2009).
[128] S. Yasui, D. Inotani, and M. Nitta, Phys. Rev. C **101**, 055806 (2020).
[129] Y. Fujimoto, K. Fukushima, and W. Weise, Phys. Rev. D **101**, 094009 (2020).
[130] Y. Fujimoto and M. Nitta, Phys. Rev. D **103**, 054002 (2021).
[131] Y. Fujimoto and M. Nitta, Phys. Rev. D **103**, 114003 (2021).
[132] Y. Fujimoto and M. Nitta, J. High Energy Phys. 09 (2021) 192.